Comparative VUV Synchrotron Excitation Study of YAG: Eu and YAG: Cr Ceramics

Amangeldy M. Zhunusbekov [1] , Zhakyp T. Karipbayev [1,*] , Akbota Tolegenova [1] , Kuat K. Kumarbekov [1], Erik E. Nurmoldin [1], Muratbek M. Baizhumanov [1] , Aleksei Kotlov [2] and Anatoli I. Popov [3,*]

1   Institute of Physical and Technical Sciences, L.N. Gumilyov Eurasian National University, Astana 010008, Kazakhstan; zhunusbekov_am@enu.kz (A.M.Z.); tulegenova93akbota@gmail.com (A.T.); kumarbekov_kk_1@enu.kz (K.K.K.); nurmoldin_yeye@enu.kz (E.E.N.); baizhumanov_mzh_1@enu.kz (M.M.B.)
2   Deutsches Elektronen-Synchrotron DESY, 22603 Hamburg, Germany; aleksei.kotlov@desy.de
3   Institute of Solid State Physics, University of Latvia, 8 Kengaraga, LV-1063 Riga, Latvia
*   Correspondence: karipbayev_zht_1@enu.kz (Z.T.K.); popov@latnet.lv (A.I.P.)

Abstract: Using synchrotron radiation, a comparative VUV excitation study of YAG ceramics doped with Eu^{3+} and Cr^{3+} ions under VUV excitation (10.5–3.7 eV) at 9 K was conducted in this work. Both ceramics exhibit distinct excitation peaks in the VUV region, indicating high-energy transitions related to the internal electronic levels of the dopants and interband transitions within the YAG matrix. For YAG:Eu, the main excitation peaks at 6–7 eV correspond to transitions within the 4f-shell of Eu^{3+} and Eu^{3+}-O^{2-} charge transfer states, showing weak dependence on the crystal field and high energy conversion efficiency. In contrast, YAG:Cr shows broad excitation bands due to transitions between levels influenced by strong crystal field interactions, resulting in lower luminescence efficiency. The study highlights the importance of crystal structure and dopant interactions in determining the spectral characteristics of YAG-based ceramics, offering potential for their application in advanced optoelectronic devices.

Keywords: yttrium luminum garnet; europium; ceramics; VUV excitation; X-ray diffractometry

1. Introduction

YAG ($Y_3Al_5O_{12}$) crystals and ceramics doped by rare-earth ions have become an important material in modern science and technology due to their unique luminescent properties [1–10]. These materials are also widely used as active laser media because of their excellent optical properties and their ability to generate intense emission at specific wavelengths [11]. They also find applications in optoelectronics, sensors, and detectors [12–14]. One of the key applications of YAG ceramics, doped with rare-earth ions is in lighting technology and scintillators [15–20]. The doping of YAG with RE ions produces materials with diverse luminescent characteristics, making them ideal for various lighting applications. As demand for these materials grows, so does the need to improve their quality characteristics, such as color rendering index (CRI). One promising material in this regard is YAG:Eu ceramics, which exhibits high energy conversion efficiency and excellent color rendering [21]. These properties make YAG:Eu ceramics an attractive material for developing high-efficiency phosphors used in LED light sources [22,23].

Most rare-earth ions absorb and emit light due to interconfigurational 4f → 5d transitions. The luminescence spectrum of the Eu^{3+} ion consists of a series of narrow bands corresponding to intra-center transitions within the f-shell. These narrow bands demonstrate a weak influence of the crystal field of the matrix on the f-shell electrons. For instance, the Eu^{3+} ion, with its $4f^6$ electronic configuration, exhibits minimal shifts in the position of its bands across different matrices [24,25]. This allows for a clear interpretation of the luminescence spectra of Re^+ ions in various materials.

Another interesting area of research involves YAG crystals and ceramics doped with chromium ions. It is important to note that chromium ions in a YAG can be in charge states +3 and/or +4 [26,27]. Because there are fundamental differences in ionic radius and valence, Cr ions are typically present as Cr^{3+} rather than Cr^{4+} to maintain valence equilibrium with substituted Al^{3+} [27]. As for trivalent chromium, such ions in YAG have an electron configuration of $3d^3$. The energy levels associated with this configuration interact strongly with the crystal field of the matrix, leading to broad spectral bands in the absorption and luminescence spectra. The energy structure of Cr^{3+} in YAG is sensitive to changes in the crystal field, allowing for control over the material's spectral characteristics through modifications of its chemical composition and structure.

Given the unique energy states of these ions in the YAG ceramic samples, the study of their luminescent characteristics when excited in the vacuum ultraviolet (VUV) region of the spectrum is of particular relevance. It is important to note, that precisely with excitation in the VUV region it is possible not only to excite high-energy states of RE, but also to study the mechanisms of energy transfer between the YAG matrix and RE, and to study the influence of crystal lattice defects on the efficiency of luminescence. Taking into account that the band gap energy value in the YAG is higher than 6.9–7.0 eV [28,29] the comprehensive study of the above processes is possible only with special VUV spectrometers and excitation sources. Therefore, among all known possibilities, synchrotron radiation is the most promising. Previous work on the VUV synchrotron excitation of luminescence of YAG samples includes YAG:Ce^{3+} nanocrystals [29], undoped YAG single crystals irradiated by 50 MeV electron beam [30], undoped, Ce^{3+} and Pr^{3+} doped YAG single crystals and films [31–33]. According [33], the band gap energy value in the YAG is between 7.85–7.95 eV, which once again confirms that the correct study of the relaxation processes of high-energy electronic excitations is possible only with the help of synchrotron radiation. Among other works, we can note the VUV studies of YAG:Yb [34] and YAG:Er [35] single crystalline films.

Research in this area opens new opportunities for the development and optimization of luminescent materials with improved properties, which is crucial for the creation of new generation LEDs, lasers, and other optoelectronic devices. VUV experiments are especially valuable for investigating these materials in the context of their potential application as scintillators. As follows from the above, the absolute majority of the research works were devoted to pure or Ce^{3+} doped samples. However, samples doped with other RE-impurities have still been practically unstudied. Therefore, the aim of this work was to study the luminescence spectra and the corresponding excitation spectra of YAG ceramics doped with rare-earth ions (Eu^{3+}) and transition metals (Cr^{3+}), which, as noted above, also play important roles in many practical applications.

2. Synthesis of Ceramics and Experimental Research Methods

Solid-state synthesis is one of the most common methods for producing YAG+ ceramics. It is based on the reaction of yttrium, aluminum, and europium oxides at high temperatures. The advantages of solid-state synthesis include its relative simplicity, availability of raw materials, and the ability to scale up the process for producing large volumes of ceramics.

$Y_3Al_5O_{12}$:Eu and $Y_3Al_5O_{12}$:Cr samples were obtained by solid-state synthesis by the authors from L.N. Gumilyov Eurasian National University. High-purity 4N yttrium (Y_2O_3), aluminum (Al_2O_3), europium (Eu_2O_3), and chromium (Cr_2O_3) oxides from Hebei Suoyi New Material Technology Co., Ltd. (Handan, China), were used as raw materials for ceramic fabrication. Fine crystalline powders of the raw materials were weighed in proportions corresponding to the required chemical composition and mixed in a stoichiometric ratio, considering the desired concentrations: for the europium-doped samples—Al_2O_3 (43%), Y_2O_3 (55%), and Eu_2O_3 (2%); and for the chromium-doped samples—Al_2O_3 (43%), Y_2O_3 (55%), and Cr_2O_3 (2%). The oxide mixture underwent mechanical processing in a ball mill for 30 min to reduce particle size and ensure a more uniform distribution of

components. The resulting batch was pressed into tablets using a hydraulic press for further synthesis.

The prepared samples were subjected to high-temperature annealing in a furnace at temperatures exceeding 1500 °C more than 6 h. As a result of the solid-state synthesis, $Y_3Al_5O_{12}$:Eu (2%) and $Y_3Al_5O_{12}$:Cr (2%) ceramics were produced. The synthesized compounds were identified using X-ray diffraction analysis (Bruker D6 PHASER). SEM and EDS analyses were performed on Tabletop Microscopes TM4000Plus II, Hitachi High-Tech Japan.

The Williamson-Hall method used to estimate the crystallite size and microstrain in materials. It is based on the assumption that the broadening of the diffraction peaks can be caused by both small crystallite size and the presence of microstrain in the crystal structure is given by: $\beta \cos \theta = (k\lambda/D) + 4\varepsilon \sin \theta$; where: β—full width at half maximum (FWHM) of the diffraction peak in radians, θ—Bragg diffraction angle, λ—wavelength of the X-ray radiation (0.15406 nm for Cu Kα), k—shape factor (~0.9 for spherical crystallites), D—average crystallite size, ε—microstrain.

Luminescence studies were carried out using synchrotron radiation at the Superlumi/P66 beamline of the PETRA III synchrotron facility at DESY in Hamburg [36]. The synchrotron radiation provided high-intensity, tunable excitation in the desired spectral range, which was selected using a 2-m monochromator with a spectral resolution of 4 Å. This ensured precise excitation of the luminescent states in the ceramic samples.

The emitted luminescence from the ceramics was detected using an ANDOR Kymera monochromator, offering a spectral resolution of 2 Å, enabling accurate detection of luminescence peaks. A Newton 920 CCD camera, Oxford Instruments, UK was employed for sensitive detection over a wide spectral range, and a Hamamatsu R6358 photomultiplier, Hamamatsu Photonics, Japan tube was used for photon counting, particularly effective in the ultraviolet range. The ceramic samples were prepared by cleaving larger pieces to obtain smooth surfaces suitable for luminescence measurements. The experiments were conducted at a temperature of 9 K using a helium-cooled cryostat to minimize thermal noise and non-radiative losses. The excitation spectra were corrected relative to the sodium salicylate signal, ensuring accurate and reliable data across the entire spectral range.

3. Experimental Results and Discussion

Figure 1 shows SEM, EDS and element mapping images of YAG:Eu and YAG:Cr ceramic samples. The provided SEM images show YAG:Eu and YAG:Cr ceramics with a magnification of $6000\times$ at a scale of 5.0 μm. These images allow the analysis of the grain structure and microdefects in ceramic materials. The YAG:Eu image shows that the grains have clear boundaries and a relatively uniform size, which can be estimated in the range of 1 to 2 μm. The grains are predominantly polygonal in shape with slight elongation in some places, no significant pores or cracks are observed, indicating a successful sintering process. Good material density indicates effective compaction during synthesis. The interaction between grains is tight, the absence of large pores indicates high quality synthesis and uniform distribution of components.

Unlike YAG:Eu, the YAG:Cr structure shows greater variability in grain sizes and shapes. Some grains are elongated, indicating uneven sintering or mechanical deformation during processing. The grain sizes vary from 0.5 to 2 μm, indicating non-uniformity of the grain structure. In the studied area, a pore or microcrack with an average size of about 2 μm can be observed. Micropores and irregularities can occur due to uneven distribution during the compaction of the batch and can also be fixed as a result of high-temperature annealing, which can fix these irregularities. Despite the presence of pores and defects, the grains have tight contact with each other, indicating a sufficient level of compaction of the material.
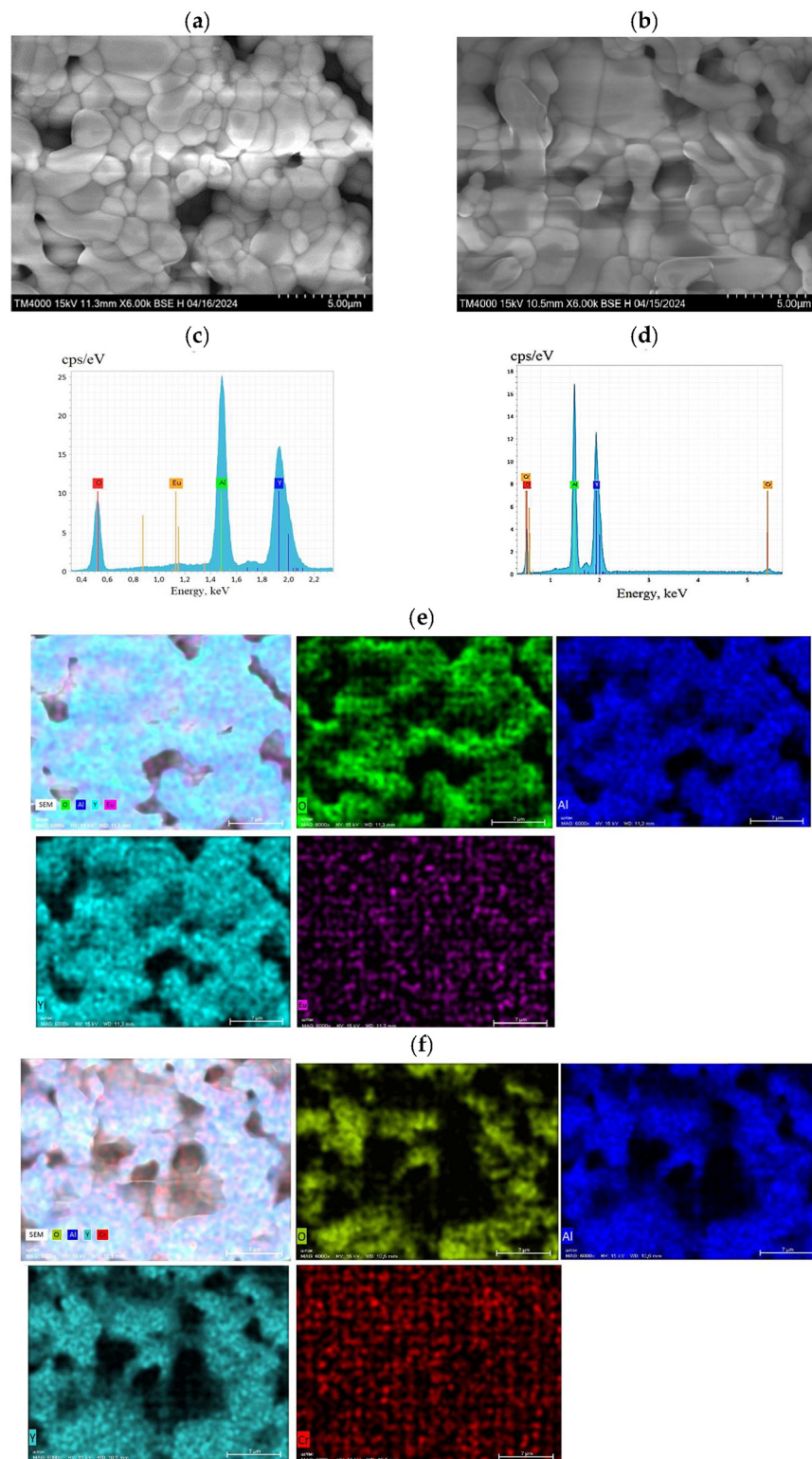
Figure 1. SEM images (**a**,**b**), EDS spectra (**c**,**d**), and element mapping images (**e**,**f**) of YAG:Eu (**a**,**c**,**e**) and YAG:Cr (**b**,**d**,**f**) ceramics.

The results of the EDS analysis are shown in Table 1. Both samples show a composition very close to the stoichiometry of $Y_3Al_5O_{12}$ (YAG). YAG:Eu: Doping with europium has minimal effect on the overall structure and the stoichiometry remains almost unchanged. The data confirms the correct distribution of yttrium, aluminum and oxygen in the structure. YAG:Cr: Although aluminum is slightly less than in YAG, yttrium compensates for this

deficit and doping with chromium slightly changes the overall stoichiometry. However, for a more accurate assessment of stoichiometry and structure, X-ray diffraction (XRD) analysis will provide clearer insights.

Table 1. Results of the EDS analysis.

Element	Line	YAG:Eu		YAG:Cr		YAG	
		Mass%	Atom%	Mass%	Atom%	Mass%	Atom%
O	K	44.98 ± 0.12	69.87 ± 0.19	43.91 ± 0.14	71.06 ± 0.22	52.6	57.9
Al	K	23.18 ± 0.06	21.35 ± 0.06	18.71 ± 0.06	17.6 ± 0.06	12.5	26.4
Y	L	30.82 ± 0.13	8.72 ± 0.04	36.96 ± 0.14	10.5 ± 0.04	34.9	16
Eu	L	1.02 ± 0.03	0.85 ± 0.01				
Cr	K			0.42 ± 0.02	0.4 ± 0.01		
Total		100.00	100.00	100.00	100.00	100.00	100.00

3.1. XRD Analysis

The Powder XRD analysis shows that the YAG sample doped with 2 wt% Eu and Cr exhibits a well-ordered structure with high-intensity diffraction peaks (Figure 2). The structure has a $Y_3Al_5O_{12}$ phase, which belongs to the cubic system. The unit cell parameters (Table 2) are a = 12.0244 Å (YAG:Eu), a = 12.0249 Å (YAG:Cr), $\alpha = 90°$, as confirmed by the ICDD database (PDF-4+ 2019, Card No00-067-0134 and No. 04-007-2667). The space group is 230 (Ia-3d), with a unit cell volume of 1747.07 Å^3 (YAG:Eu) and 1738.78 Å^3 (YAG:Cr) and a calculated phase density of 4.514 (YAG:Eu) and 4.535 g/cm^3 (YAG:Cr). The diffractogram demonstrated that the solid-phase method produced a ceramic with a high degree of crystallinity and excellent structural characteristics. In addition to the garnet phase, a secondary phase of perovskite (YAlO$_3$) was detected in small quantities. The perovskite phase exhibited unit cell parameters of a = 5.178 Å, b = 5.324 Å, c = 7.374 Å for YAG:Eu, with an orthorhombic symmetry corresponding to the space group Pbnm (ICDD card No. 04-015-5193). Due to the low content of the perovskite phase (7.4% for YAG:Eu), its crystallite size 23.4 nm, unit cell volumes were calculated as 203.31 Å^3. Although the YAG:Eu ceramics contain a perovskite phase, the luminescence spectral characteristics reveal typical properties of the YAG phase, as detailed below.
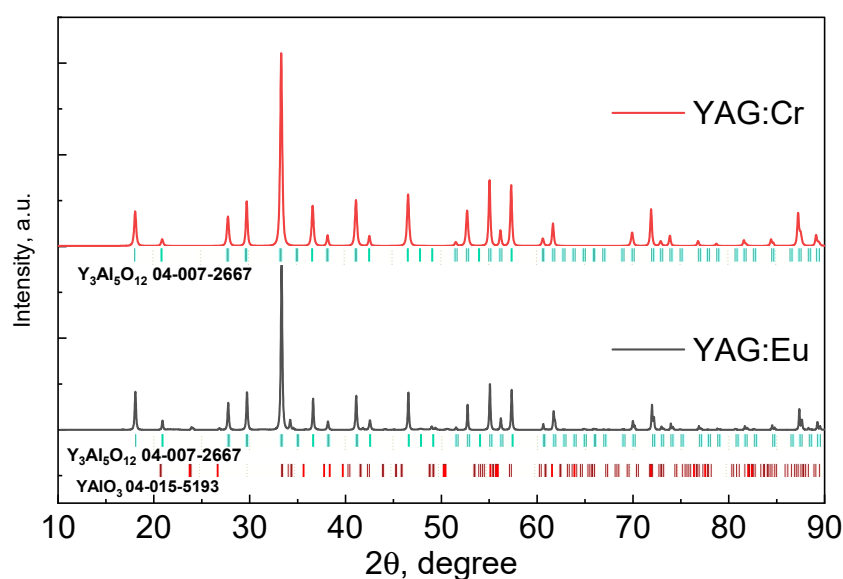

Figure 2. Diffraction patterns of YAG:Eu and YAG:Cr ceramics.

Table 2. Crystal lattice parameters for synthesized ceramics.

Sample	Phase Name	Content, %	a (Å)	b (Å)	c (Å)	α (deg)	V (Å³)	Space Group	DB Card Number	Crystallite Size (nm)
YAG:Eu	yttrium aluminum garnet, $Y_3A_5O_{12}$	92.6	12.044 ± 0.002			90	1747.07 ± 4.15	230 : Ia-3d	04-007-2667	27.5
	perovskite group, $YAlO_3$	7.4	5.334 ± 0.002	7.407± 0.002	5.205± 0.002	90	205.88 ± 4.15	62 : Pbnm	04-015-5193	23.4
YAG:Cr	yttrium aluminum garnet, $Y_3A_5O_{12}$	92.1	12.0249 ± 0.002			90	1738.77 ± 4.15	230 : Ia-3d	04-007-2667	38.8

The main diffraction peaks are located at 2θ angles given in (Table 3) characterized by high intensities and narrow widths. The crystallite size, determined using the Williamson-Hall method, was 38.88 nm (YAG:Cr) and 27.5 nm (YAG:Eu), indicating a high-quality structure with minimal lattice strain, amounting to only 0.115%. These results confirm that the synthesized YAG:Eu and YAG: Cr ceramics has high stability and structural order.

Table 3. Position of diffraction peaks and FWHM (deg) of YAG:Eu and YAG:Cr ceramics.

	YAG:Eu				YAG:Cr	
No.	2-Theta (deg)	FWHM (deg)	(hkl)	Phase Name	2-Theta (deg)	FWHM (deg)
1	18.228	0.196	2,1,1	$Y_3Al_5O_{12}$	18.062	0.214
2	21.083	0.231	(2,2,0), (1,0,1)	$Y_3Al_5O_{12}$, $YAlO_3$	20.872	0.234
3	24.20	0.221	1,1,0	$YAlO_3$		
4	24.331	0.381	0,0,2	$YAlO_3$		
5	27.009	0.181	1,1,1	$YAlO_3$		
6	27.912	0.212	3,2,1	$Y_3Al_5O_{12}$	27.739	0.210
7	29.843	0.230	4,0,0	$Y_3Al_5O_{12}$	29.996	0.093
8	33.482	0.198	4,2,0	$Y_3Al_5O_{12}$	33.283	0.187
9	34.395	0.205	1,1,2	$YAlO_3$		
10	34.762	0.210	2,0,0	$YAlO_3$		
11	35.233	0.343	3,3,2	$Y_3Al_5O_{12}$		
12	36.754	0.201	4,2,2	$Y_3Al_5O_{12}$	36.557	0.185
13	38.317	0.197	4,3,1	$Y_3Al_5O_{12}$	38.117	0.185
14	40.755	0.222	1,0,3	$YAlO_3$		
15	41.270	0.204	5,2,1	$Y_3Al_5O_{12}$	41.060	0.184
16	41.929	0.278	0,2,2	$YAlO_3$	42.463	0.176
17	42.707	0.201	(4,4,0), (2,0,2)	$Y_3Al_5O_{12}$, $YAlO_3$	42.749	0.102
18	44.286	0.185	1,1,3	YAlO3	43.256	0.157
19	45.667	0.154	1,2,2	YAlO3		
20	46.684	0.209	5,3,2	Y3Al5O12	46.492	0.180
21	49.166	0.241	(5,4,1), (2,2,0)	$Y_3Al_5O_{12}$, $YAlO_3$		
22	49.519	0.209	0,0,4	$YAlO_3$		
23	50.771	0.323	0,2,3	$YAlO_3$		
24	51.684	0.176	6,3,1	$Y_3Al_5O_{12}$	51.489	0.198
25	52.939	0.233	4,4,4	$Y_3Al_5O_{12}$	52.674	0.182
26	54.277	0.069	2,1,3	$YAlO_3$		

Table 3. *Cont.*

	YAG:Eu				YAG:Cr	
No.	2-Theta (deg)	FWHM (deg)	(hkl)	Phase Name	2-Theta (deg)	FWHM (deg)
27	55.193	0.209	6,4,0	$Y_3Al_5O_{12}$	55.004	0.178
28	55.742	0.709	2,2,2	$YAlO_3$		
29	56.313	0.207	(7,2,1), (1,3,1)	$Y_3Al_5O_{12}$, $YAlO_3$	56.147	0.175
30	57.472	0.222	(6,4,2), (3,1,1)	$Y_3Al_5O_{12}$, $YAlO_3$	57.267	0.176
31	60.736	0.240	(6,5,1), (1,3,2,)	$Y_3Al_5O_{12}$, $YAlO_3$	60.565	0.183
32	61.258	0.243	0,2,4	$YAlO_3$		
33	61.881	0.216	(8,0,0), (2,0,4)	$Y_3Al_5O_{12}$, $YAlO_3$	61.646	0.183
34	62.797	0.272	(7,4,1), (2,2,3)	$Y_3Al_5O_{12}$, $YAlO_3$	62.706	0.153
35	64.999	0.173	(6,5,3), (2,3,1)	$Y_3Al_5O_{12}$, $YAlO_3$	64.775	0.184
36	66.025	0.189	(6,6,0), (1,0,5)	$Y_3Al_5O_{12}$, $YAlO_3$	65.819	0.159
37	67.633	0.212	1,3,3	$YAlO_3$		
38	68.364	0.223	1,1,5	$YAlO_3$	68.87	0.173
39	69.103	0.162	(7,5,2), (2,3,2)	$Y_3Al_5O_{12}$, $YAlO_3$		
40	69.909	0.255	3,2,2	$YAlO_3$	69.907	0.186
41	70.095	0.188	8,4,0	$Y_3Al_5O_{12}$	71.891	0.176
42	72.091	0.226	(8,4,2), (0,4,1)	$Y_3Al_5O_{12}$, $YAlO_3$	72.895	0.179
43	73.109	0.197	(7,6,1), (4,0,0)	$Y_3Al_5O_{12}$, $YAlO_3$	73.864	0.174
44	74.073	0.192	6,6,4	$Y_3Al_5O_{12}$		
45	74.973	0.143	8,5,1	$Y_3Al_5O_{12}$	74.842	0.189
46	76.997	0.238	(9,3,2), (1,3,4)	$Y_3Al_5O_{12}$, $YAlO_3$	76.783	0.176
47	77.911	0.284	(8,4,4), (0,0,6)	$Y_3Al_5O_{12}$, $YAlO_3$	77.840	0.144
48	78.348	0.184	4,0,2	$YAlO_3$		
49	78.877	0.225	9,4,1	$Y3Al5O12$	78.713	0.185
50	80.853	0.213	(10,1,1), (4,1,2)	$Y_3Al_5O_{12}$, $YAlO_3$	80.634	0.170
51	81.769	0.219	10,2,0	$Y_3Al_5O_{12}$	81.575	0.171
52	82.501	0.201	(9,4,3), (0,4,3)	$Y_3Al_5O_{12}$, $YAlO_3$		
53	83.774	0.112	2,2,5	$YAlO_3$		
54	84.146	0.193	4,2,1	$YAlO_3$		
55	84.613	0.210	(10,3,1), (2,3,4)	$Y_3Al_5O_{12}$, $YAlO_3$	84.427	0.186
56	87.433	0.206	(10,4,0), (0,2,6)	$Y_3Al_5O_{12}$, $YAlO_3$	87.254	0.186
57	88.213	0.493	(9,6,1), (2,0,6)	$Y_3Al_5O_{12}$, $YAlO_3$	88.189	0.179
58	89.311	0.192	(10,4,2), (3,1,5)	$Y_3Al_5O_{12}$, $YAlO_3$	89.131	0.197

3.2. Luminescence of YAG:Eu and YAG:Cr Ceramics

The intrinsic luminescence band of YAG in YAG:Eu and YAG:Cr ceramics, when excited in the excitonic absorption region at 6.69, and another energy 7.5, 8.25 eV, is shown in Figure 3a. The broad emission band with a maximum at 377 nm corresponds to defects within the both ceramics (Figure 3a inset). The primary types of defects typically present in such wide-bandgap oxide dielectrics as YAG include oxygen vacancies, antisite defects (AD), which relate to lattice site disorder, and various uncontrolled impurities. In reference [37], the intrinsic luminescence of YAG single crystals is clearly associated with radiative recombination at Y_{Al} antisite defects.
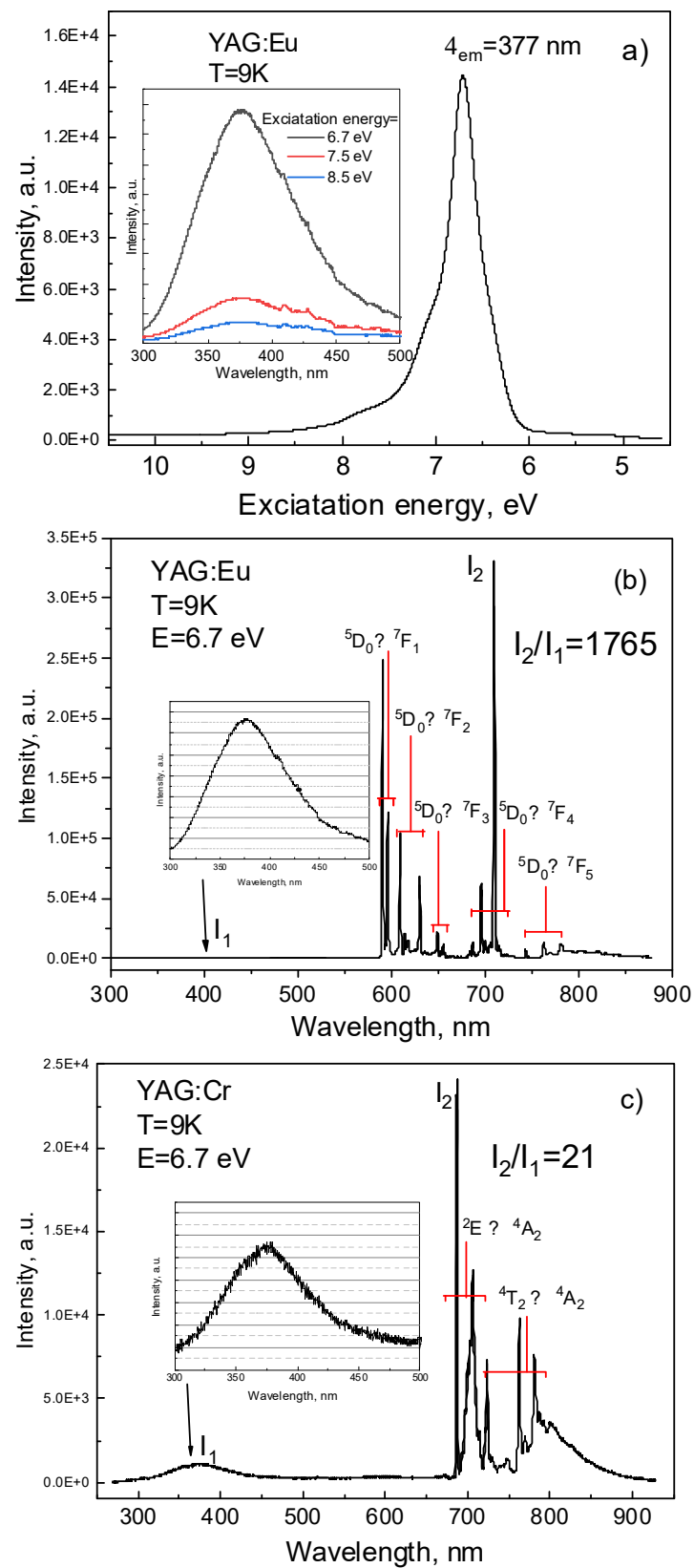
Figure 3. Luminescence excitation spectrum recorded at 377 nm (**a**); in the inset (**a**) emission spectra at 6.7, 7.5 and 8.5 eV. (**b**,**c**) emission spectra at 6.7 eV; in the inset (**b**,**c**) emission spectra at 6.7 eV.

Studies [38,39] have shown that, in YAG-based ceramics, the intrinsic luminescence band shifts towards the longer wavelength region of the spectrum, with a peak around

390 nm. Additionally, the emission typically observed at approximately 300 nm in single crystals is absent in ceramics. This emission is attributed to excitons localized near Y_{Al} antisite defects or to recombination luminescence occurring around such defects. The absence of the 300 nm emission band suggests that such defects are likely absent in the ceramics, possibly due to the lower synthesis temperature compared to the growth of single crystals from high-temperature melts. Figure 4 shows the excitation spectrum of the luminescence for the emission maximum at 380 nm. The luminescence excitation spectrum peaks at 6.69 eV, corresponding to the transition through the bandgap (Eg), confirming the intrinsic luminescence of YAG.
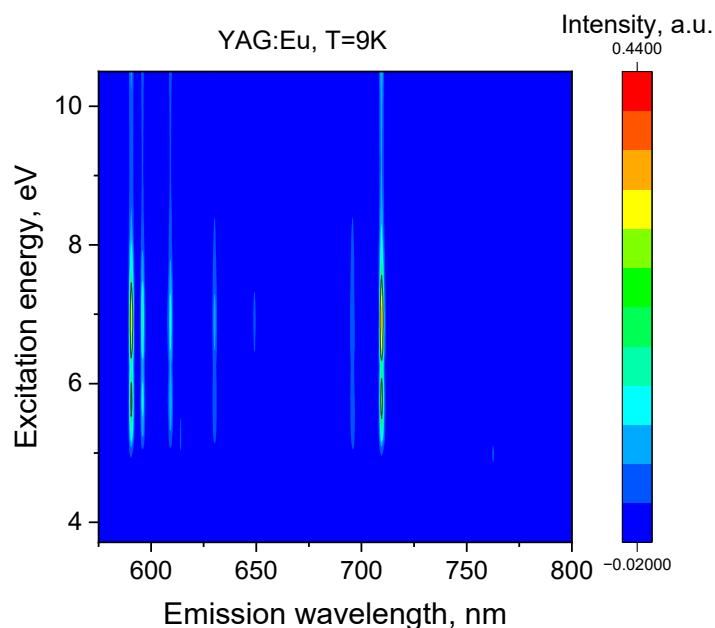
Figure 4. 3D excitation/emission mapping of YAG:Eu ceramic.

Figure 3b,c present the luminescence spectra in the 300–900 nm range under excitation at 6.7 eV. The ratios of the intensities of intrinsic luminescence, with a maximum at 380 nm, to impurity luminescence in the region of 600–800 nm are shown. For the ceramics YAG:Eu and YAG:Cr, the ratio between impurity and intrinsic luminescence was 1765 and 21, respectively. These differences in the impurity-to-intrinsic luminescence ratios between YAG:Eu and YAG:Cr reflect disparities in the luminescent properties of the dopant ions. In YAG:Eu, the impurity luminescence due to Eu^{3+} ions significantly surpasses the intrinsic luminescence of the matrix owing to the high efficiency of energy absorption and emission. In contrast, in YAG:Cr, the impurity luminescence from Cr^{3+} ions is less pronounced, leading to a lower intensity ratio. However, in both ceramics, the impurity luminescence remains intense. These differences are highlighted to compare energy transfer efficiency to impurity centers and the degree of competition with intrinsic defects under near-excitonic excitation or excitations above the bandgap width.

3.2.1. YAG:Eu

The presented (Figure 4) 3D excitation/emission mapping of YAG:Eu ceramic, conducted at a temperature of 9 K, shows the dependence of luminescence intensity on excitation energy (on the vertical axis) and emission wavelength (on the horizontal axis). The intense peaks on the mapping indicate resonant transitions at certain excitation energies, most pronounced at around 6–7 eV. The correlation between excitation energy and emission wavelength reflects the specificity of excited electronic states in Eu^{3+} ions. The mapping reveals the complex interaction of europium ions within the YAG crystal lattice. The optical transitions are associated with internal d-f and f-f transitions in Eu^{3+} ions.

Figure 5 shows the luminescence spectra of YAG:Eu ceramics with excitation under 6.9, 7.5 and 8.25 eV. The obtained spectra showed narrow-line $^5D_n-^7F_m$ luminescence of Eu^{3+} ions [40].
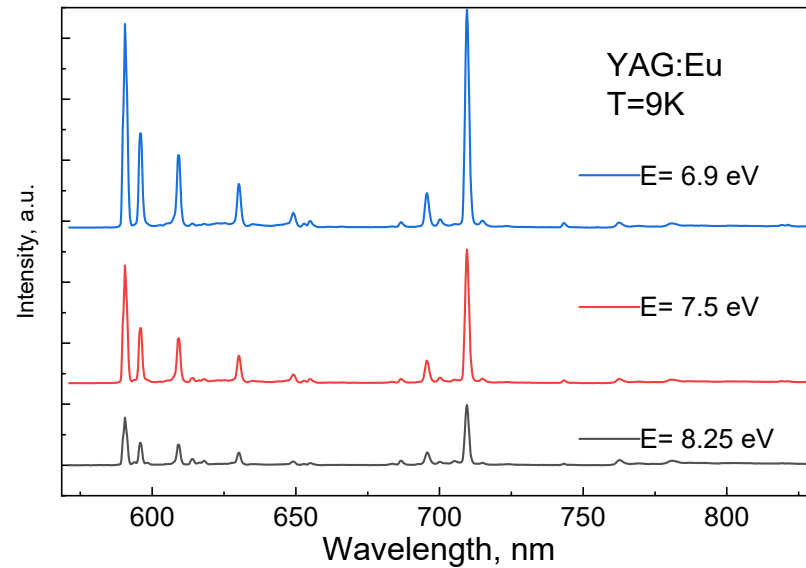

Figure 5. Luminescence spectrum of YAG:Eu ceramics under 6.9, 7.5 and 8.25 eV excitation.

The spectrum consists of several bands of different intensities corresponding to transitions from the $^5D_0$ level. The most intense line with a maximum at a wavelength of 709 nm is observed for the $^5D_0-^7F_4$ transition. In this wavelength region, there are also several weak maxima with 695, 740, and 762 nm wavelengths. Sufficiently intense lines are observed at wavelengths of 590 and 595 nm, which corresponds to the $^5D_0-^7F_1$ transition, as well as at wavelengths of 609 and 630 nm, which corresponds to the $^5D_0-^7F_2$ transition. The lowest intensity is the $^5D_0-^7F_3$ transition with maxima at 649 and 654 nm, 740 and 762 nm lines are due to the $^5D_0-^7F_5$ transition. Figure 6 shows the normalized luminescence excitation spectra for several emission bands. The excitation spectrum does not change for all emission maxima.
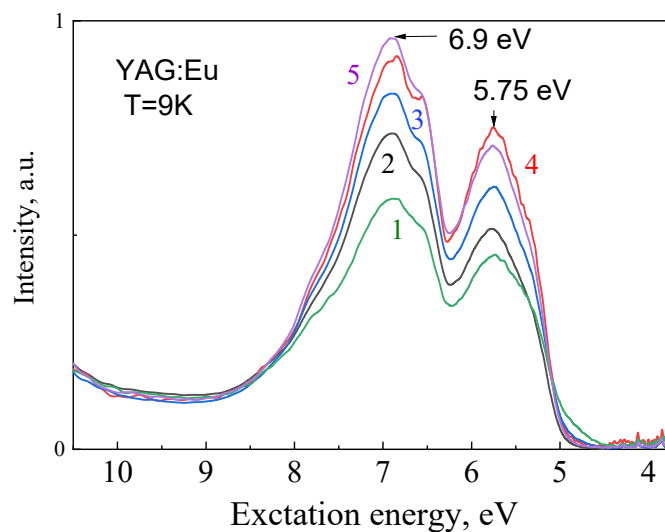
Figure 6. Normalized luminescence excitation spectra measured at different emission peaks: 1—695 nm, 2—709 nm, 3—590 nm, 4—610 nm, 5—596 nm.

The excitation spectra for the emission bands at 590, 596, 610, 695 and 710 nm, as well as the luminescence spectrum of YAG:Eu ceramics, are shown in Figure 6. The main excitation band of intrinsic emission, as seen, corresponds to the exciton transition at 6.77 eV. In the excitation spectra recorded at the emission maxima of the Eu^{3+} ion, a broad band with peaks at 6.89 eV nm and 6.64 eV is observed. It is known that energy absorption resulting from the exciton transition (7 eV) in a doped crystal may involve two mechanisms of excitation energy relaxation. These mechanisms include charge transfer transitions and transitions between the f and d electronic levels of the europium ion (Eu^{3+}). In the case of YAG, the charge transfer process involves the electron transition between the Eu^{3+} ion and oxygen ions in the matrix Eu^{3+}-O^{2-} [41]. This may lead to the formation of transient Eu^{2+} states and an increase in oxygen vacancies. The difference in the excitation spectra at the registration maxima of 380 nm and 590 nm shows that light absorption can occur at these transitions, which contributes to the excitation of electrons in the crystal lattice.

The energy position of the charge transfer state (CTS) of Eu^{3+} is associated with the covalent bond between Eu^{3+} and O^{2-}, and the symmetry number of Eu^{3+}. The higher the covalence of the Eu^{3+}-O^{2-} bond, the lower the energy position will be. Figure 7 shows the energy transition scheme corresponding to the different maxima in the excitation spectra (curve 2), and a luminescence maximum of Eu^{3+} is observed at 6.64 eV, which is associated with the charge transfer process. The second excitation region between 4.28 and 6.86 eV contains several weak sharp peaks related to the f–f electronic transitions of Eu^{3+} ions, with maxima at 300 and 321 nm ($^7F_0$–^5L_J), which corresponds to [41].
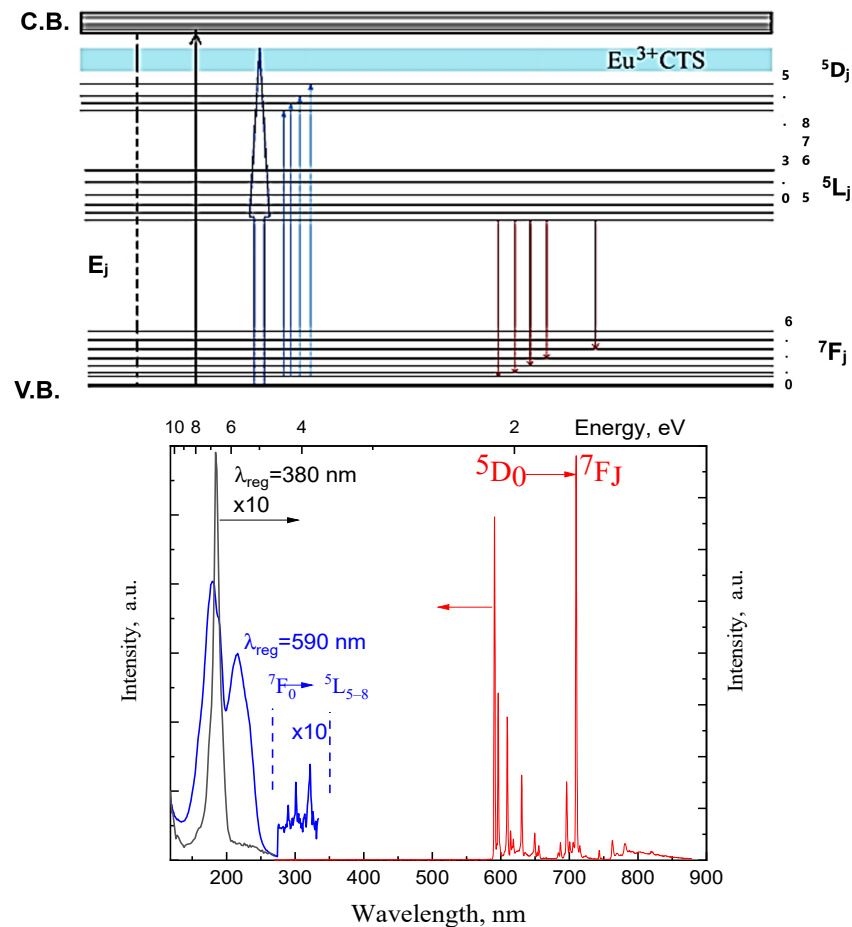

Figure 7. Scheme of energy transitions in the Eu^{3+} ion in the YAG matrix and excitation and luminescence spectra for YAG:Eu. CTS of Eu^{3+}-O^{2-}.

3.2.2. YAG:Cr

As is well known, the Cr^{3+} ion has an electron configuration of d^3. In the absence of an external field, the electrons can occupy any of the five possible d orbitals. However, when the Cr^{3+} ion interacts with the crystal field of YAG, the d orbitals undergo energy splitting, resulting in the formation of the $^4A_2$, ^2E and $^4T_2$ levels. This splitting significantly affects the optical and other physical properties of the ion, which is crucial in materials science. Due to this, YAG ceramics doped with chromium (Cr^{3+}) exhibit unique luminescent properties, making them promising materials for various practical applications.

The luminescence spectra of YAG:Cr ceramics were also measured at a temperature of 9 K under VUV excitation. In the presented Figure 8, the 3D excitation/emission mapping for YAG:Cr ceramics at 9 K shows the dependence of luminescence intensity on excitation energy (vertical axis) and emission wavelength (horizontal axis). Excitation in the range of 6 to 8 eV leads to the appearance of intense luminescent bands, indicating strong optical transitions. The horizontal axis represents the emission wavelengths from 680 to 800 nm. The most intense luminescence bands are concentrated around 700–720 nm, which are associated with characteristic transitions in Cr^{3+} ions within the YAG crystal lattice.
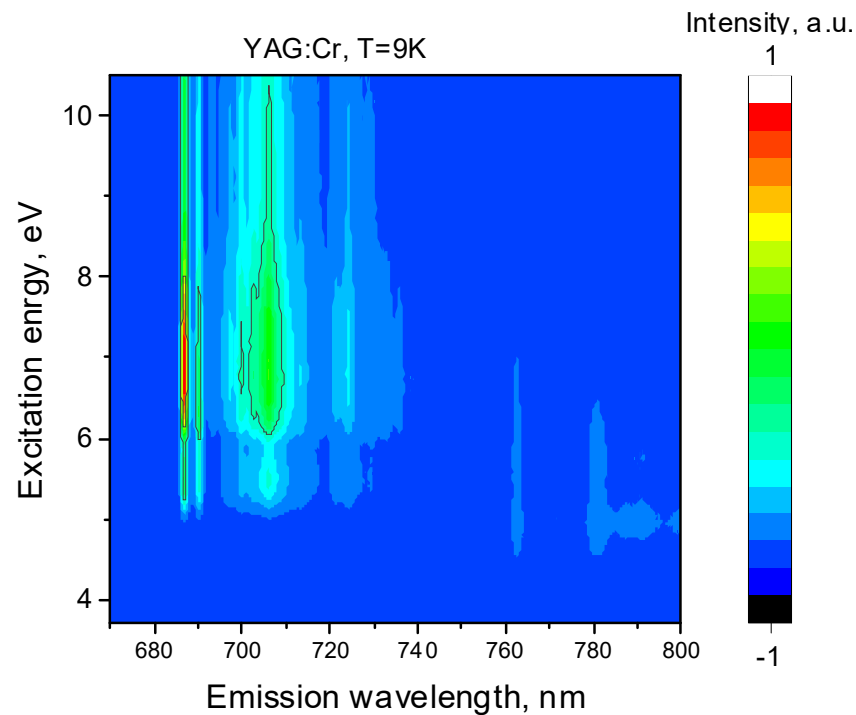

Figure 8. 3D excitation/emission mapping of YAG:Cr ceramic.

Figure 9 shows the luminescence spectrum under 6.9, 7.5 and 8.25 eV excitation. The spectrum consists of a narrow R-line at a wavelength of 688 nm and several bands at 690, 706, 724, 762, and 780 nm. The primary luminescence mechanism (688–724 nm) for Cr^{3+} ions in the YAG matrix is associated with transitions between the ^2E and $^4A_2$ states. The long-wavelength bands at 762–800 nm are related to transitions between the $^4T_2 \rightarrow {}^4A_2$ states [42]. These transitions occur at lower energies compared to the $^2E \rightarrow {}^4A_2$ transitions and are responsible for the longer-wavelength emissions.
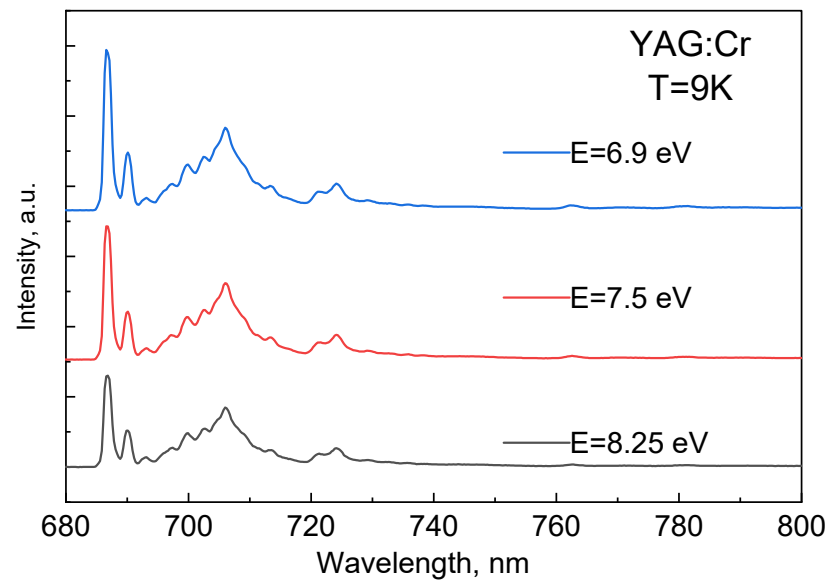
Figure 9. Luminescence spectrum of YAG:Cr ceramics excitation under 6.9, 7.5 and 8.25 eV at 9 K.

This detailed emission behavior highlights the optical properties of Cr^{3+} ions and their potential for various practical applications, particularly in fields requiring materials with specific luminescent properties at low temperatures.

The excitation spectra (Figure 10) revealed several distinct peaks, the most prominent at 6.76 eV, 5.5 eV, and 4.95 eV. These peaks indicate energy transitions in Cr^{3+} ions embedded in the YAG matrix. The highest intensity is observed at an excitation energy of 6.76 eV for all emission wavelengths, corresponding to an interband transition in the YAG matrix. The peak at 5.5 eV is likely associated with transitions within the 3d-shell of Cr^{3+} ions, which are influenced by their interaction with the YAG crystal field. Similarly, the peak at 4.95 eV may indicate transitions between states affected by the octahedral crystal field. Thus, the observed peaks reflect the complex interplay between Cr^{3+} ions and the crystalline structure of the YAG matrix, impacting the energy levels and the nature of the transitions. The excitation spectra for 686, 704, and 723 nm follow a similar trend. The distinction lies in the excitation spectrum at 786 nm, which is associated with differences in the excitation mechanisms and transitions involved in the luminescence of Cr^{3+} ions in the YAG matrix. It is well known that under the influence of an octahedral crystal field, the d orbitals of Cr^{3+} ions split into two sets of energy levels, which are responsible for radiative transitions. The similarity of the excitation spectra for the peaks at 686–724 nm is related to $^2E \rightarrow {}^4A_2$ transitions, which share identical excitation and relaxation pathways.

In [43], the relationship between increasing concentrations of Cr^{3+} ions in the octahedral positions of the YAG crystal lattice and changes in the intensity of the crystal field is detailed. The weakening of the crystal field causes a redshift of the transitions. It is hypothesized that the difference in the VUV excitation spectra for the peaks at 762 and 780 nm, compared to the R-lines, is related to distinct interactions with the crystal field. In this case, the $^4T_2 \rightarrow {}^4A_2$ transition is predominant.

Thus, the YAG matrix and the octahedral environment of Cr^{3+} ions play a crucial role in determining the excitation spectra. The interaction between the crystal field and the d-orbitals of Cr^{3+} ions lead to different energy levels and transitions. In particular, the narrow luminescence lines associated with the $^2E \rightarrow {}^4A_2$ transitions indicate strong interaction with the crystal field, while the broader bands corresponding to the $^4T_2 \rightarrow {}^4A_2$ transitions suggest a weaker interaction.
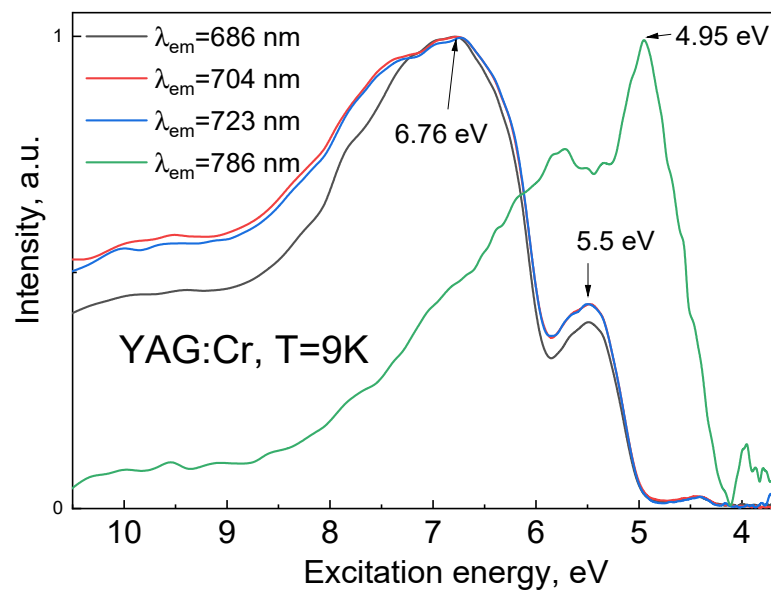
Figure 10. Luminescence excitation spectra at 686, 704, 723 and 786 nm at 9 K.

Before drawing a conclusion, it should be noted that the efficiency of energy transfer during the final excitation of impurity luminescent ions depends significantly on the presence of point defects, many of which are created under the influence of hard radiation of particles (fast ions, protons, neutron and/or electrons). Such radiation defects have been well studied in various garnets [44–50] However, their role in energy transfer processes is still practically unexplored. In a subsequent paper, we will report on the role of fast heavy ion irradiation on the luminescent characteristics of YAG crystals and ceramics.

4. Conclusions

Samples of YAG:Eu and YAG:Cr were obtained using the solid-state synthesis method. For both types of ceramics, pronounced excitation peaks in the VUV region are characteristic, indicating high-energy transitions associated with the internal electronic levels of the dopants and interband transitions in the YAG matrix.

The main excitation peaks of YAG are located in the range of 6–7 eV and are related to transitions within the 4f-shell of Eu^{3+} and charge transfer states of Eu^{3+}-O^{2-}. The spectra demonstrate a weak dependence on the crystal field of the ion matrix, resulting in narrow spectral lines. A high energy conversion efficiency is observed, indicating effective absorption and emission of energy by Eu^{3+} ions.

In the excitation spectra of YAG:Cr, broad bands appear, which are caused by transitions between levels affected by strong interaction with the crystal field. This leads to a broad spectral energy distribution and lower luminescence efficiency compared to YAG:Eu. Significant differences in excitation spectra at various wavelengths (especially in the 786 nm region) indicate more complex transition mechanisms and competition between radiative and non-radiative processes. The crystal field of the YAG matrix has a strong influence on the energy levels of Cr^{3+} ions, causing their splitting and the formation of multiple transitions with varying intensities. In the case of Eu^{3+} ions, this influence is minimal, as evidenced by narrow spectral bands and slight energy shifts. Optimizing synthesis conditions and controlling composition allow for the tuning of their luminescent characteristics, providing opportunities for the development of new materials with improved properties.

These conclusions highlight the importance of crystal structure and interaction with dopants in determining the spectral characteristics of YAG-based ceramic materials and their potential for further development and application in high-tech devices.

References

1. Zorenko, Y.; Zych, E.; Voloshinovskii, A. Intrinsic and Ce^{3+}-related luminescence of YAG and YAG: Ce single crystals, single crystalline films and nanopowders. *Opt. Mater.* **2009**, *31*, 1845–1848. [CrossRef]
2. Zorenko, Y.; Mares, J.A.; Kucerkova, R.; Gorbenko, V.; Savchun, V.; Voznyak, T.; Nikl, M.; Beitlerova, A.; Jurek, K. Optical, luminescence and scintillation characteristics of Bi-doped LuAG and YAG single crystalline films. *J. Phys. D Appl. Phys.* **2009**, *42*, 075501. [CrossRef]
3. Zorenko, Y.; Zorenko, T.; Gorbenko, V.V.; Voznyak, T.; Savchyn, V.; Bilski, P.; Twardak, A. Peculiarities of luminescent and scintillation properties of YAG: Ce phosphor prepared in different crystalline forms. *Opt. Mater.* **2012**, *34*, 1314–1319. [CrossRef]
4. Valiev, D.; Han, T.; Stepanov, S.; Vaganov, V.; Paygin, V. The effect of BaF2 concentration and particle size distribution on the luminescence efficiency of YAG: Ce^{3+} phosphors. *Mater. Res. Express* **2018**, *5*, 096201. [CrossRef]
5. Han, T.; Lang, T.; Zhong, Y.; Cao, S.; Peng, L.; Yakovlev, A.; Polisadova, E. Spectral broadening of a single Ce^{3+}-doped garnet by chemical unit cosubstitution for near ultraviolet LED. *Opt. Mater. Express* **2018**, *8*, 3761–3769. [CrossRef]
6. Polisadova, E.; Valiev, D.; Vaganov, V.; Oleshko, V.; Tao, H.; Zhang, C.; Burachenko, A.; Popov, A.I. Time-resolved cathodoluminescence spectroscopy of YAG and YAG:Ce^{3+} phosphors. *Opt. Mater.* **2019**, *96*, 109289. [CrossRef]
7. Karipbayev, Z.T.; Lisitsyn, V.M.; Mussakhanov, D.A.; Alpyssova, G.K.; Popov, A.I.; Polisadova, E.F.; Elsts, E.; Akilbekov, A.T.; Kukenova, A.B.; Kemere, M.; et al. Time-resolved luminescence of YAG:Ce and YAGG:Ce ceramics prepared by electron beam assisted synthesis. *Nucl. Instrum. Methods Phys. Res. B* **2020**, *479*, 222–228. [CrossRef]
8. Chaika, M.A.; Tomala, R.; Strek, W. Infrared laser stimulated broadband white emission of transparent Cr: YAG ceramics obtained by solid state reaction sintering. *Opt. Mater.* **2021**, *111*, 110673. [CrossRef]
9. Pankratov, V.; Pankratova, V.; Popov, A.I. Luminescence and vacuum ultraviolet excitation spectroscopy of nanophosphors under synchrotron irradiation. *Phys. Status Solidi* **2022**, *259*, 2100475. [CrossRef]
10. Karipbayev, Z.T.; Lisitsyn, V.M.; Golkovski, M.G.; Zhilgildinov, Z.S.; Popov, A.I.; Zhunusbekov, A.M.; Polisadova, E.; Tulegenova, A.; Mussakhanov, D.A.; Alpyssova, G.; et al. Electron Beam-Assisted Synthesis of YAG:Ce Ceramics. *Materials* **2023**, *16*, 4102. [CrossRef]
11. Morris, J.A.; Pollock, C.R. Passive Q switching of a diode-pumped Nd: YAG laser with a saturable absorber. *Opt. Lett.* **1990**, *15*, 440–442. [CrossRef]
12. Nilsson, S.; Feuk, H.; Richter, M. High temperature thermographic phosphors YAG: Tm; Li and YAG: Dy in reduced oxygen environments. *J. Lumin.* **2023**, *256*, 119645. [CrossRef]
13. Jedoń, J.; Zych, E.; Zeler, J.; Gorbenko, V.; Zorenko, Y. YAG: Tb@ YAG: Pr single crystalline dual-layer phosphor. An alternative approach to multimodal wide range luminescence thermometry. *Adv. Opt. Mater.* **2024**, *12*, 2303284. [CrossRef]
14. Sevic, D.; Krizan, J.; Rabasovic, M.S.; Marinkovic, B.P. Temperature sensing using YAG: Dy single-crystal phosphor. *Eur. Phys. J. D* **2021**, *75*, 56. [CrossRef]
15. Basaif, A.; Oresegun, A.; Zubair, H.T.; Zin, H.; Choo, K.Y.; Ibrahim, S.A.; Wang, T.; Wen, J.; Gang, D.; Lewis, E.; et al. Time-resolved radiation dosimetry using a cerium and terbium Co-doped YAG crystal scintillator. *Radiat. Phys. Chem.* **2023**, *204*, 110625. [CrossRef]
16. Zapadlík, O.; Nikl, M.; Polák, J.; Průša, P.; Linhart, V. Engineering of YAG: Ce to improve its scintillation properties. *Opt. Mater. X* **2022**, *15*, 100165.

17. Dormenev, V.; Brinkmann, K.T.; Borisevich, A.; Kazlou, D.; Korzhik, M.; Moritz, M.; Novotny, R.W.; Orsich, P.; Gerasymov, I.; Tkachenko, S.; et al. Radiation tolerant YAG: Ce scintillation crystals grown under reducing Ar$^+$ CO atmosphere. *Nucl. Instrum. Methods Phys. Res. Sect. A* **2021**, *1015*, 165764. [CrossRef]

18. Zahra, B.; Guerbous, L.; Bousbia-Salah, H.; Boukerika, A. Effect of Ce^{3+} Content and Annealing Temperature on the Optical and Scintillation Properties of Ce^{3+}-Doped Y$_3$Al$_5$O$_{12}$ Nanoscintillator Synthesized by Sol–Gel Route. *Phys. Status Solidi (A)* **2023**, *220*, 2300022. [CrossRef]

19. Pankratova, V.; Butikova, J.; Kotlov, A.; Popov, A.I.; Pankratov, V. Influence of swift heavy ions irradiation on optical and luminescence properties of Y$_3$Al$_5$O$_{12}$ single crystals. *Opt. Mater. X* **2024**, *23*, 100341. [CrossRef]

20. Pankratova, V.; Skuratov, V.A.; Buzanov, O.A.; Mololkin, A.A.; Kozlova, A.P.; Kotlov, A.; Popov, A.; Pankratov, V. Radiation effects in Gd$_3$(Al, Ga)$_5$: O12: Ce^{3+} single crystals induced by swift heavy ions. *Opt. Mater. X* **2022**, *16*, 100217. [CrossRef]

21. Yao, J.; Zhu, Q.; Li, J.G. Garnet transparent ceramic film of Y$_3$Al$_5$O$_{12}$: Eu^{3+} fabricated through an interface reaction of layered rare-earth hydroxide nanosheets on amorphous alumina. *Appl. Surf. Sci.* **2022**, *579*, 152226. [CrossRef]

22. Sharma, P.K.; Dutta, R.K.; Pandey, A.C. Performance of YAG: Eu^{3+}, YAG: Tb^{3+} and BAM: Eu^{2+} plasma display nanophosphors. *J. Nanoparticle Res.* **2012**, *14*, 731. [CrossRef]

23. Ravichandran, D.; Roy, R.; Chakhovskoi, A.A.; Hunt, C.E.; White, W.B.; Erdei, S. Fabrication of Y$_3$Al$_5$O$_{12}$: Eu thin films and powders for field emission display applications. *J. Lumin.* **1997**, *71*, 291–297. [CrossRef]

24. Görller-Walrand, C.; Binnemans, K. Chapter 167 Spectral Intensities of f-f Transitions. In *Handbook on the Physics and Chemistry of Rare Earths*; Elsevier: Amsterdam, The Netherlands, 1998; Volume 3, pp. 101–264. [CrossRef]

25. Binnemans, K. Interpretation of Europium(III) Spectra. *Coord. Chem. Rev.* **2015**, *295*, 1–45. [CrossRef]

26. Dong, J.; Deng, P.; Xu, J. Spectral and luminescence properties of Cr^{4+} and Yb^{3+} ions in yttrium aluminum garnet (YAG). *Opt. Mater.* **2000**, *14*, 109–113. [CrossRef]

27. Ma, B.; Zhang, W.; Luo, H.; Yuan, F.; Cheng, B.; Bai, L.; Tang, Y.; Song, H.Z. Growth of Cr, Yb: YAG single crystals for self-Q-switched monolithic solid-state lasers. *Opt. Mater.* **2023**, *143*, 114218. [CrossRef]

28. Zych, E.; Brecher, C.; Glodo, J. Kinetics of cerium emission in a YAG: Ce single crystal: The role of traps. *J. Phys. Condens. Matter.* **2000**, *12*, 1947. [CrossRef]

29. Tanner, P.A.; Fu, L.; Ning, L.; Cheng, B.M.; Brik, M.G. Soft synthesis and vacuum ultraviolet spectra of YAG: Ce^{3+} nanocrystals: Reassignment of Ce^{3+} energy levels. *J. Phys. Condens. Matter.* **2007**, *19*, 216213. [CrossRef]

30. Aleksanyan, E.; Kirm, M.; Vielhauer, S.; Harutyunyan, V. Investigation of luminescence processes in YAG single crystals irradiated by 50 MeV electron beam. *Radiat. Meas.* **2013**, *56*, 54–57. [CrossRef]

31. Zorenko, Y.; Voloshinovskii, A.; Savchyn, V.; Voznyak, T.; Nikl, M.; Nejezchleb, K.; Spassky, D. Exciton and antisite defect-related luminescence in Lu$_3$Al$_5$O$_{12}$ and Y$_3$Al$_5$O$_{12}$ garnets. *Phys. Status Solidi* **2007**, *244*, 2180–2189. [CrossRef]

32. Zorenko, Y.; Gorbenko, V.; Mihokova, E.; Nikl, M.; Nejezchleb, K.; Vedda, A.; Spassky, D. Single crystalline film scintillators based on Ce-and Pr-doped aluminium garnets. *Radiat. Meas.* **2007**, *42*, 521–527. [CrossRef]

33. Zorenko, T.; Gorbenko, V.; Nizankovskiy, S.; Zorenko, Y. Comparison of the luminescent properties of Y$_3$Al$_5$O$_{12}$: Pr crystals and films. *Acta Phys. Pol. A* **2018**, *133*, 948–953. [CrossRef]

34. Zorenko, Y.; Zorenko, T.; Gorbenko, V.; Voznyak, T.; Popielarski, P.; Batentschuk, M.; Fedorov, A. Luminescent properties of LuAG:Yb and YAG:Yb single crystalline films grown by Liquid Phase Epitaxy method. *Radiat. Meas.* **2016**, *90*, 132–135. [CrossRef]

35. Zorenko, Y.; Gorbenko, V.; Zorenko, T.; Savchyn, V.; Batentschuk, M.; Osvet, A.; Brabec, C. Luminescent properties and energy transfer processes in YAG: Er single crystalline films. *J. Lumin.* **2014**, *154*, 198–203. [CrossRef]

36. Omelkov, S.I.; Chernenko, K.; Ekström, J.C.; Jurgilaitis, A.; Khadiev, A.; Kivimäki, A.; Kirm, M. Recent advances in time-resolved luminescence spectroscopy at MAX IV and PETRA III storage rings. *J. Phys. Conf. Ser.* **2022**, *2380*, 012135. [CrossRef]

37. Zorenko, Y.; Voloshinovskii, A.; Konstankevych, I.; Kolobanov, V.; Mikhailin, V.; Spassky, D. Luminescence of Excitons and Antisite Defects in the Phosphors Based on Garnet Compounds. *Radiat. Meas.* **2004**, *38*, 677–680. [CrossRef]

38. Zych, E.; Brecher, C.; Lingertat, H. Host-Associated Luminescence from YAG Optical Ceramics under Gamma and Optical Excitation. *J. Lumin.* **1998**, *78*, 121–134. [CrossRef]

39. Zych, E.; Brecher, C. Temperature Dependence of Host-Associated Luminescence from YAG Transparent Ceramic Material. *J. Lumin.* **2000**, *90*, 89–99. [CrossRef]

40. Orekhova, K.; Tomala, R.; Zamoryanskaya, M. The Study of Composition, Structure and Cathodoluminescent Features of YAG:Eu^{3+} Nanoceramics. Excitation Capture Efficiency of Eu^{3+} Energy Levels. *J. Alloys Compd.* **2021**, *858*, 157731. [CrossRef]

41. Kolesnikov, I.E.; Tolstikova, D.V.; Kurochkin, A.V.; Manshina, A.A.; Mikhailov, M.D. Eu3+ Concentration Effect on Luminescence Properties of YAG:Eu^{3+} Nanoparticles. *Opt. Mater.* **2014**, *37*, 306–310. [CrossRef]

42. Dantelle, G.; Reita, V.; Ibanez, A.; Ledoux, G.; Dujardin, C. Luminescent Nd3+, Cr3+ Codoped YAG Nanocrystals for Thermal Sensing: Influence of the Excitation Wavelength. *Phys. B Condens. Matter* **2022**, *628*, 413622. [CrossRef]

43. Chen, X.; Lu, T.; Wei, N.; Lu, Z.; Chen, L.; Zhang, Q.; Cheng, G.; Qi, J. Fabrication and Photoluminescence Properties of Cr:YAG and Yb,Cr:YAG Transparent Ceramic. *Opt. Mater.* **2015**, *49*, 330–336. [CrossRef]

44. Pujats, A.; Springis, M. The F-type centres in YAG crystals. *Radiat. Eff. Defects Solids* **2001**, *155*, 65–69. [CrossRef]

45. Zorenko, Y.; Zorenko, T.; Voznyak, T.; Mandowski, A.; Xia, Q.; Batentschuk, M.; Friedrich, J. Luminescence of F+ and F centers in AI$_2$O$_3$-Y$_2$O$_3$ oxide compounds. In *IOP Conference Series: Materials Science and Engineering*; IOP Publishing: Bristol, UK, 2010; Volume 15, p. 012060.

46. Karipbayev, Z.T.; Kumarbekov, K.; Manika, I.; Dauletbekova, A.; Kozlovskiy, A.L.; Sugak, D.; Popov, A.I. Optical, structural, and mechanical properties of $Gd_3Ga_5O_{12}$ single crystals irradiated with ^{84}Kr+ ions. *Phys. Status Solidi* **2022**, *259*, 2100415. [CrossRef]
47. Babin, V.; Laguta, V.V.; Maaroos, A.; Makhov, A.; Nikl, M.; Zazubovich, S. Luminescence of F^+-type centers in undoped $Lu_3Al_5O_{12}$ single crystals. *Phys. Status Solidi (b)* **2011**, *248*, 239–242. [CrossRef]
48. Meng, F.; Wu, Y.; Koschan, M.; Melcher, C.L.; Cohen, P. Effect of annealing atmosphere on the cerium valence state and F^+ luminescence center in Ca-codoped GGAG: Ce single crystals. *Phys. Status Solidi* **2015**, *252*, 1394–1401. [CrossRef]
49. Mironova-Ulmane, N.; Popov, A.I.; Antuzevics, A.; Krieke, G.; Elsts, E.; Vasil'chenko, E.; Sildos, I.; Puust, L.; Ubizskii, S.B.; Sugak, D.; et al. EPR and optical spectroscopy of neutron-irradiated $Gd_3Ga_5O_{12}$ single crystals. *Nucl. Instrum. Methods Phys. Res. Sect. B Beam Interact. Mater. At.* **2020**, *480*, 22–26. [CrossRef]
50. Jia, L.; Zhu, J.; Boyaryntseva, Y.; Gerasymov, I.; Grynyov, B.; Sidletskiy, O. Effect of Carbon Doping on F-Type Defects in YAG and YAG: Ce Crystals. *Phys. Status Solidi* **2021**, *258*, 2100325. [CrossRef]